

Possibility of resonant capture of antiprotons by highly charged hydrogenlike ions

M. Genkin^a and E. Lindroth

Dept. of Atomic Physics, Stockholm University, 10691 Stockholm, Sweden

Received 23 October 2008 / Received in final form 1st December 2008

Published online 29 January 2009 – © EDP Sciences, Società Italiana di Fisica, Springer-Verlag 2009

Abstract. Recently, an experimental setup was proposed by Lapierre et al. [*Physics with ultra slow antiproton beams*, *AIP Conference Proceedings* (2005), Vol. 793, p. 361] which would allow antiprotons and highly charged ions to collide repeatedly in an electron beam ion trap (EBIT) due to a nested trap configuration. As mentioned by the authors, such a setup may open the possibility to study antiproton capture into well-defined states through a resonant process which involves simultaneous electron excitation. In the present work, we give some theoretical estimations of the feasibility of that process.

PACS. 36.10.-k Exotic atoms and molecules (containing mesons, antiprotons and other unusual particles) – 32.80.Zb Autoionization

1 Introduction

Exotic atoms are fascinating systems where the parameters determining the properties of ordinary matter can be tuned and investigated in completely new regimes. As a consequence these systems can often be used as test benches for fundamental constants and symmetries. For example, the studies of metastable states in antiprotonic Helium recently lead to a new and much improved value for the electron-antiproton mass ratio [2,3]. That value can be translated to a determination of the proton-antiproton mass ratio, i.e. to a test of CPT symmetry. The antiprotonic systems studied so far [4–17] are produced when antiprotons are stopped in liquids or gases. A slow antiproton can then replace one of the atomic (A) electrons (occupying the main quantum number n_e) through the process $A + \bar{p} \rightarrow A^+ \bar{p} + e$, where it will enter into a state with main quantum number $n \approx n_e \sqrt{\mu_p / \mu_e}$.

With the planned Facility for Low-Energy Antiproton and Ion Research (FLAIR) at GSI, Germany, cooled antiprotonic beams of an intensity many orders of magnitude larger than available today will be provided. This might open new possibilities for the production of antiprotonic exotic systems. As mentioned in [1], a nested trap configuration, e.g. based on the electron beam ion trap at the Max Planck Institute in Heidelberg, Germany (HD-EBIT), would eventually, if combined with an antiproton source of sufficient intensity, allow to search for a process that can be seen as the antiprotonic analogon of the resonant process of dielectronic recombination. If, in an antiproton-ion collision, the energy of the antiproton $\epsilon_{\bar{p}}$ is

tuned such that the resonant condition is fulfilled, a target electron can be excited and a doubly excited electron-antiproton state may form

$$A^{q+} + \bar{p} \rightarrow [A^{q+} \bar{p}]^{**} \quad (1)$$

where q is the charge of the ion A . The doubly excited electron-antiproton state can subsequently decay by electron, antiproton or photon emission, and the different decay rates will essentially determine the cross section for antiprotonic capture. This process would, if probable enough, provide an excellent possibility for high precision spectroscopy of antiprotonic ions, since the capture occurs in a well defined state that can be controlled by tuning the collision energy. In this work, we aim to investigate the formation and decay channels of such a state in order to obtain a theoretical estimation of its feasibility. For simplicity, we restrict ourselves to collisions with highly charged hydrogenlike ions with the electron being in the ground state.

The present article is structured as follows. In Section 2, we schematically describe possible decay channels for resonant antiproton capture and present a way to estimate the cross section. The computational methods are given in Section 3 and some illustrative calculations for an example ion are shown in Section 4. In the last section, the validity and restrictions on the chosen approach are discussed, followed by some concluding remarks. Atomic units are used throughout unless stated otherwise.

^a e-mail: genkin@physto.se

2 Theory

2.1 Decay channels

The doubly excited state $[A^{q+}\bar{p}]^{**}(nl)_e(n'l')_{\bar{p}}$ formed in the collision (1) is lying above the ground state of A^{q+} . We now give a qualitative description of its decay channels:

$$[A^{q+}\bar{p}]^{**}(nl)_e(n'l')_{\bar{p}} \rightarrow A^{q+}(1s)_e + \bar{p} \quad (2)$$

referred to as antiproton ejection in the following,

$$[A^{q+}\bar{p}]^{**}(nl)_e(n'l')_{\bar{p}} \rightarrow [A^{(q+1)+}\bar{p}](n' - \Delta n' l' - \Delta l')_{\bar{p}} + e \quad (3)$$

referred to as Auger electron emission, and finally also electronic and antiprotonic radiative dipole transitions:

$$[A^{q+}\bar{p}]^{**}(nl)_e(n'l')_{\bar{p}} \rightarrow [A^{q+}\bar{p}](n - \Delta n l \pm 1)_e(n'l')_{\bar{p}} + \gamma, \quad (4)$$

$$[A^{q+}\bar{p}]^{**}(nl)_e(n'l')_{\bar{p}} \rightarrow [A^{q+}\bar{p}](nl)_e(n' - \Delta n' l' \pm 1)_{\bar{p}} + \gamma, \quad (5)$$

here and in the following n, n', l, l' denote the approximate one particle quantum numbers. Note that the formation of the doubly excited state (1) is the time reverse of antiproton ejection (2) and hence the rates should be the same according to the principle of detailed balance. While the process (2) leads to the loss of the antiproton, Auger electron emission and radiative transitions can be seen as stabilization channels since the antiproton is bound in the final state. Finally, we remark that the additional process of direct radiative capture can be neglected in the present context since it results dominantly in antiproton capture into low lying states (this can be seen for example from Kramers formula [18]) close to the nucleus. This would lead to fast annihilation of the antiproton so that no precise spectroscopy of the exotic system can be performed.

2.2 Estimation of the cross section

In dielectronic recombination calculations it is common to describe the cross section of an isolated resonance by a Lorentz profile as in e.g. [19,20]:

$$\sigma(\epsilon) = \frac{1}{\pi} S \frac{\Gamma/2}{(E_d - E_i - \epsilon)^2 + \Gamma^2/4}, \quad (6)$$

where E_d is the energy of the doubly excited state, E_i the initial energy of the target ion (simply given by the 1s orbital energy in our case) and ϵ the positive energy of the incoming particle. This description is known to be adequate for resonances with a width much smaller than the distance from the nearest threshold. Clearly, the profile has its maximum at $\epsilon = E_d - E_i$. The width of the doubly excited state is denoted by Γ and S is the recombination strength of the process, i.e. the integrated cross section

$$S = \int \sigma(\epsilon) d\epsilon. \quad (7)$$

Since the described mechanism for antiprotonic capture is very similar to dielectronic recombination, there is no reason to abandon this picture. Some modifications, however, are indeed necessary. The dielectronic recombination process usually denotes the complete two-step mechanism, where a continuum electron is captured by simultaneous excitation of a core electron to form a doubly excited state (first step), and subsequent stabilization by photoemission (second step) to complete the recombination. The recombination strength can be expressed through the autoionization rate A_a of the doubly excited state (which is the inverse process of its formation) and the total radiative rate A_r (i.e. the sum over all possible radiative channels) and is proportional to $S \sim A_a A_r / (A_a + A_r)$ because the emission of a photon is the only possible stabilization channel when the particles are indistinguishable. Furthermore, if the rates differ by some orders of magnitude, the faster one can be neglected in the fraction and S is simply proportional to the slowest rate (this is often the case in light systems, where $S \sim A_r$). In the present case, the first step is very similar to dielectronic recombination, but the stabilization is more complex. When the system decays by particle emission, we have to differentiate between antiproton, equation (2), and electron emission, equation (3) in the doubly excited state, and since the electron emission provides an additional stabilization channel it should be included in the expression for S , which with all factors reads

$$S = \frac{\hbar^3 \pi^2}{2\mu_{\bar{p}}(E_d - E_i)} \frac{g_d}{g_i} \frac{A_a \sum A_{\text{stab}}}{A_a + \sum A_{\text{stab}}}. \quad (8)$$

Here, the sum over all stabilization channels, $\sum A_{\text{stab}}$, includes now the total radiative rate and the rate for all electron emission channels and A_a is the antiproton ejection rate which corresponds to autoionization in dielectronic recombination. The weight factors g_d and g_i stand for the multiplicity of the doubly excited state and of the initial ion respectively. We can conclude that for a quantitative treatment of the process the calculations of the rates of the different decay channels is indispensable.

3 Computational methods

Essentially, one has to calculate the positions and widths of the resonances as well as the radiative transition rates. The widths occur due to the coupling to the continuum through the electron-antiproton interaction and can be determined together with their positions by means of complex rotation. The radiative rates can be obtained within the dipole approximation, as briefly described below.

3.1 Complex rotation

The technique of complex rotation has proven to be a powerful tool for the description of resonances in atomic systems during the last decades. It has also recently been applied to antiprotonic helium [21]. Its advantage, obtained by rotating the Hamiltonian eigenvalue problem into the

complex plane, is that it allows a simultaneous calculation of the positions, E_r , and the widths, Γ , of the resonances from the complex eigenvalues, E , of the complex symmetric Hamiltonian matrix

$$E = E_r - i\Gamma/2. \quad (9)$$

The non-relativistic three-body Hamiltonian of the system in the center of mass frame reads

$$H = \frac{p_e^2}{2\mu_e} + \frac{p_{\bar{p}}^2}{2\mu_{\bar{p}}} + \frac{\mathbf{p}_e \cdot \mathbf{p}_{\bar{p}}}{m_N} - \frac{e^2}{4\pi\epsilon_0} \left(\frac{Z}{r_e} + \frac{Z}{r_{\bar{p}}} - \frac{1}{r_{12}} \right), \quad (10)$$

where Z is the nuclear charge, μ_e and $\mu_{\bar{p}}$ denote the reduced masses of the electron and antiproton (and m_N the mass of the nucleus), r_e and $r_{\bar{p}}$ their distance to the nucleus and $r_{12} = |\mathbf{r}_e - \mathbf{r}_{\bar{p}}|$ the distance between them. The kinetic energy of the nucleus is accounted for through the use of reduced masses in the first two terms and the inclusion of the term $\mathbf{p}_e \cdot \mathbf{p}_{\bar{p}}/m_N$, referred to as mass polarization in the following.

We set up the Hamiltonian matrix in a basis of hydrogenlike product wave functions

$$|\phi_{ab}^{SL\pi}\rangle = |\{n_a l_a n_b l_b\} SL\pi\rangle, \quad (11)$$

where S is the total spin, L is the total angular momentum and π is the parity. The one-particle hydrogenlike orbitals can be obtained efficiently through B -Splines, which are piecewise polynomial functions defined on a given set of points, referred to as a knot sequence, distributed in a certain interval. B -Splines have several desirable properties [22] and are widely used in physical applications (see e.g. [23] for an overview). The solutions to the hydrogenlike one-particle Hamiltonian,

$$h(r) = -\frac{\hbar^2}{2\mu} \frac{\partial^2}{\partial r^2} + \frac{l(l+1)\hbar^2}{2\mu r^2} - \frac{Ze^2}{4\pi\epsilon_0 r}, \quad (12)$$

are expanded as

$$P_{nl}(r) = \sum_i c_i B_i(r), \quad (13)$$

where the coefficients c_i are obtained by solving the eigenvalue equation given by the projection of the Hamiltonian in equation (12) onto the B -Spline set. Complex scaling of the radial coordinate ($r \rightarrow r \exp(i\theta)$) with a real rotation angle $0 \leq \theta \leq \pi/4$ is introduced in equation (12) by multiplying the kinetic energy term with $\exp(-2i\theta)$ and the potential energy term with $\exp(-i\theta)$.

The two-particle Hamiltonian (10) can be written as

$$H = h_e + h_{\bar{p}} + h_{12} \quad (14)$$

where h_e and $h_{\bar{p}}$ have the form as in equation (12) (with $r = r_e, r_{\bar{p}}$, $\mu = \mu_e, \mu_{\bar{p}}$) and

$$h_{12} = \frac{\mathbf{p}_e \cdot \mathbf{p}_{\bar{p}}}{m_N} + \frac{e^2}{4\pi\epsilon_0 r_{12}} \quad (15)$$

where the contributions to the kinetic and potential energy are scaled as before. Now each matrix element of

H in the basis (11) can be calculated, yielding a complex symmetric Hamiltonian matrix. After diagonalization, the energies of the resonances are obtained in the form given in (9). The whole procedure follows closely that of references [24,25].

3.2 Radiative transitions

We use the first order perturbation approach in the dipole approximation where the radiative rate A_r for a transition from an initial state $|\psi_i\rangle$ to a final state $|\psi_f\rangle$ is in first order given by

$$A_r = \frac{1}{4\pi\epsilon_0} \frac{4}{3\hbar^4} \left(\frac{\Delta E}{c} \right)^3 |\langle \psi_f | E1 | \psi_i \rangle|^2, \quad (16)$$

here, ΔE is the energy difference between the initial and the final state and $E1$ is the dipole transition operator. The final state $|\psi_f\rangle$ is approximated by a product state of the antiprotonic and electronic one-particle orbitals. For a highly charged ion this gives sufficient accuracy. Even in light exotic systems such as antiprotonic helium this approximation can be used [26], although corrections to the energy clearly become more important [27].

4 Illustrative calculations

As an illustration, we will investigate a few chosen resonances in a collision of antiprotons with a medium heavy hydrogenlike ion, Ca^{19+} . The high charge simplifies the calculations, since the correlation between the electron and the antiproton is rather weak in this case. (This does not hold for very light systems – antiprotonic helium shows strong molecular features where e.g. a Born-Oppenheimer treatment is suitable [28].) On the other hand, the ion is light enough so that a non-relativistic treatment is meaningful. The decisive quantity for the process studied here is, as will be shown later, the capture rate into the doubly excited state which to a first approximation is independent of nuclear charge. The results presented can thus be generalized to neighboring ions, at least for a qualitative picture. The calculated structure of the positions of the resonances for a total angular momentum of $L = 12$ (see below) is schematically shown in Figure 1. All resonances arising from the $n_e = 2$, $n_{\bar{p}} = 48$ configurations lie below the $1s$ threshold, apart from one. The latter one, however, lies very close to the threshold. Such resonances are known to be very hard to describe numerically, and no reliable results for the width were obtained in this work. The resonances arising from the $n_e = 3$, $n_{\bar{p}} = 45$ and $n_e = 4$, $n_{\bar{p}} = 44$ configurations lie very densely and could not be resolved properly. The isolated resonance approach (6) may not be valid in this case. Further, if the aim is to be able to control which state the antiproton is captured into an isolated resonance is more appropriate. Thus, we focus on resonances with their main contribution from the $n_e = 2$, $n_{\bar{p}} = 49$ configurations in the following illustrative calculations.

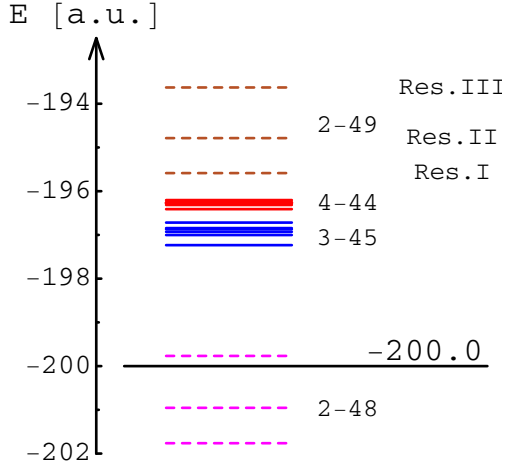


Fig. 1. (Color online) Calculated structure of the electron-antiproton resonances in hydrogenlike calcium at fixed total angular momentum $L = 12$ (this choice will be motivated in Sect. 4.1). The dashed lines indicate resonances arising from contributions with $n_e = 2$, while solid lines denote resonances from higher electronic states ($n_e = 3, 4$). The numbers 44, 45, 48, 49 are the main quantum numbers of the contributing one-particle antiprotonic orbitals $n_{\bar{p}}$. The $1s$ threshold of Ca^{19+} is at -200 a.u.

4.1 Angular momentum dependence and validation

The described combination of complex rotation with B -Splines and subsequent diagonalization of the complex matrix (also known as complex scaled configuration interaction CSCI) has already been applied to multiply excited electronic states (see e.g. [25]). However, when applying the same method to doubly excited electron-antiproton states one is confronted with some practical difficulties due to the fast oscillations of the high- n antiprotonic states and the different extensions of the antiprotonic and the electronic wave functions. To handle this situation we work with different knot sequences for the two particles. The number of knot points N_k^e used for the electronic functions is $N_k^e = 45$ with a box size of 2.0 a.u. and two different choices were tested for the antiprotonic functions ($N_k^{\bar{p}} = 275$ and $N_k^{\bar{p}} = 325$) with a box size of 0.2 a.u. The electronic knot sequence is linear in the beginning and exponential further out. This is a scheme that is well tested. The distance between the knots in the antiprotonic sequence is on the other hand slowly and steadily increasing to obtain roughly the same number of knots between the nodes in the $n = 49$ states for the full extension of the wave function. The needed number of B -Splines is estimated through comparison of the numerically calculated energies of the relevant hydrogenlike one-particle orbitals with the analytical values, that is, $N_k^{\bar{p}}$ is increased until a sufficiently good agreement is achieved. For example, the analytical value of the antiprotonic $n = 49$ orbital is $E = -149.1940989$ a.u., and the numerically obtained values are $E = -149.194087$ a.u. (with $N_k^{\bar{p}} = 275$) and $E = -149.1940985$ a.u. (with $N_k^{\bar{p}} = 325$).

In order to further check the method for numerical stability, we calculate now some relevant quantities with

analytical wave functions and compare those with the corresponding result obtained with our method. This also allows us to analyze the role of the total angular momentum, as will be discussed below.

As the next step in the validation procedure we calculate the antiproton ejection rate for a single product state in the framework of the Fermi *golden rule* and compare with the one obtained with complex rotation. In the framework of the former, a decay rate A (or the corresponding width $\Gamma = \hbar A$) for a transition from an initial state $|\psi_i\rangle$ to a final state $|\psi_f\rangle$ caused by an interaction U is given by

$$\Gamma = 2\pi\rho|\langle\psi_f|U|\psi_i\rangle|^2, \quad (17)$$

where ρ denotes the density of states. For the antiproton emission from a doubly excited electron-antiproton state, U can be approximated by the Coulomb interaction between the particles ($U = (r_{12})^{-1}$ in atomic units). For further simplification, we represent the final state by a single product wave function of the electronic $1s$ orbital and the antiprotonic regular Coulomb function with an energy ϵ and angular momentum L which is also the total angular momentum of the system

$$|\psi_f\rangle = |\{1s \epsilon L\}L\rangle. \quad (18)$$

The initial doubly excited state can be represented in the basis (11), and since the total spin and parity are unaffected by the Coulomb interaction we can write

$$|\psi_i\rangle = \sum_{a,b} c_{ab} |\{n_a l_a n_b l_b\}L\rangle \quad (19)$$

where a, b run over all fixed parity combinations for which l_a and l_b can be coupled to L . The main contribution will come from the dominating basis functions (with $n_a = 2$ and $n_b = 49$), that is, from the matrix elements of the form

$$\begin{aligned} &\langle\{1s \epsilon L\}L|(r_{12})^{-1}|\{2s 49 L\}L\rangle, \\ &\langle\{1s \epsilon L\}L|(r_{12})^{-1}|\{2p 49 L \pm 1\}L\rangle. \end{aligned} \quad (20)$$

They can be explicitly written as

$$\begin{aligned} &\langle\{n_a l_a \epsilon l_b\}L|(r_{12})^{-1}|\{n_c l_c n_d l_d\}L\rangle = \\ &\sum_{k=0}^{\infty} R^k (-1)^{l_b+l_c+L} \left\{ \begin{matrix} l_a & l_b & L \\ l_d & l_c & k \end{matrix} \right\} \langle l_a || \mathcal{C}^k || l_c \rangle \langle l_b || \mathcal{C}^k || l_d \rangle \end{aligned} \quad (21)$$

where we introduced the standard notation for Wigner $6j$ -symbols and reduced matrix elements between spherical tensor operators \mathcal{C}^k [29], representing the angular part, while R^k stands for the radial part of the integral

$$R^k = \int dr_1 dr_2 P_{n_a l_a}(r_1) F_{\epsilon \bar{p}}^{l_b}(r_2) \frac{r_1^k}{r_{>}^{k+1}} P_{n_c l_c}(r_1) P_{n_d l_d}(r_2) \quad (22)$$

where we denote the Coulomb wave with energy ϵ and angular momentum l_b by $F_{\epsilon}^{l_b}$ and by P_{nl} the bound state reduced radial wave function, which are all known analytically. For a stable implementation of Coulomb functions, Barnett's algorithm was used [30]. To investigate

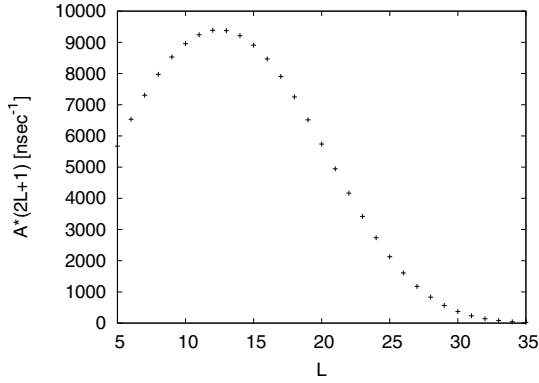


Fig. 2. Multiplicity scaled squared matrix element $A = 2\pi|\langle\{1s \epsilon L\}L|(r_{12})^{-1}|\{2s 49 L\}L\rangle|^2$ converted to inverse time units as a function of the total angular momentum L at fixed energy $\epsilon = 4.95$ a.u. (see text for further details). The energy equals approximately the difference between the $1s$ threshold at -200 a.u. and the position of the considered resonances. However, it should be stated that for slightly different energies the matrix elements are practically identical.

the angular momentum dependence we restrict ourselves to the first matrix element in (20) with $l_a = l_c = 0$ and $l_b = l_d = L$ (see (21)). Here, the angular part equals unity and only the $k = 0$ term in the sum contributes. The results of the calculation are shown in Figure 2. It turns out that the squared matrix element is indeed very sensitive to the total angular momentum and can vary by several orders of magnitude (similar behaviour is also found for the other matrix elements listed in (20)). If we also account for the multiplicity, the recombination strength (8) is proportional to $g_d A_d$ and has its maximum around $L = 12$. This motivates our choice of angular momentum (cf. caption of Fig. 1).

We can now compare the transition rate calculated with Fermi *golden rule* and analytical wave functions for a single product state with the width obtained as the imaginary part of the complex scaled *second-order* energy contribution, which should be identical. We look thus for the equality

$$\pi|\langle\{1s \epsilon 12\}12|(r_{12})^{-1}|\{2s 49 12\}12\rangle|^2 = -\text{Im} \left[\sum_{i=1}^{N^{\bar{p}}} \frac{\langle\{1s i 12\}12|(r_{12})^{-1}|\{2s 49 12\}12\rangle^2}{E_{2s}^e + E_{49,12}^{\bar{p}} - E_{1s}^e - E_i} \right]_{r \rightarrow r \exp(i\theta)} \quad (23)$$

The sum on the right hand side runs over the whole spectrum of the antiprotonic radial functions i (with the corresponding energies E_i) generated with B -Splines and $N^{\bar{p}}$ is the number of the states included (which is limited by the chosen B -Spline parameters). The energy ϵ of the Coulomb wave on the left hand side equals the term $\epsilon = E_{2p}^e + E_{49,12}^{\bar{p}} - E_{1s}^e = 0.812$ a.u. that appears in the denominator on the right hand side. Note however that the energies E_i are complex and thus the condition $\epsilon \neq E_i$ holds for all i in (23). As shown in Figure 3 agreement is achieved for a sufficient number of included configura-

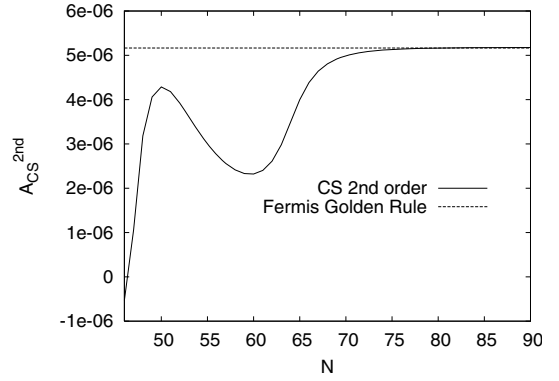


Fig. 3. Convergence of expression (23) as a function of the number of included antiprotonic states $N^{\bar{p}}$ (here $N_{\text{max}}^{\bar{p}} = N_k^{\bar{p}} - k - 2 = 316$) for the matrix element $A = \pi|\langle\{1s \epsilon 12\}12|(r_{12})^{-1}|\{2s 49 12\}12\rangle|^2$. All values are given in atomic units.

tions (the relative difference between the analytical value and the converged result is about 10^{-4}). A similarly good agreement is found also for the other matrix elements. This comparison provides, in fact, two kinds of information: the agreement between the analytical value and the sum in (23) can be seen as an indicator of how well the antiprotonic wave functions are represented by the B -Splines (i.e. if the used number of knot points $N_k^{\bar{p}}$ is sufficient), while how fast (that is, after how many included terms) the sum converges towards the analytical expression is a measure at which point it can be truncated. As can be seen from the figure, already after $N^{\bar{p}} \approx 85$ terms convergence is provided, although the number of knot points in the antiprotonic knot sequence $N_k^{\bar{p}}$ would allow to include $N_{\text{max}}^{\bar{p}} = N_k^{\bar{p}} - k - 2 = 316$ antiprotonic states. However, one should keep in mind that the results given so far do not even approximately give the true antiproton ejection rate since we considered only one particular basis state instead of a coherent sum. Nevertheless, the scaling with respect to total angular momentum could be investigated and the numerical accuracy was tested.

4.2 Rates

The number of configurations that can be included in a full CSCI calculation in practice is, of course, limited by the computational resources and the basis set needs to be truncated in some way. After performing some convergence tests, the following configuration have been used. We restricted the angular symmetries to $\{s, L\}$ and $\{p, L \pm 1\}$, while the maximum number of antiprotonic orbitals is limited by the used B -Splines parameters as $N_k^{\bar{p}} - k - 2 = 316$ where $N_k^{\bar{p}} = 325$ is the number of knot points used and $k = 7$ the order of the B -Splines. The same restriction applies to the number of electronic orbitals, for the representation of which $N_k^e = 45$ knot-points were used and hence $N_{\text{max}} = 36$. However, to keep the size of the matrix to be diagonalized within reasonable boundaries we truncated the antiprotonic basis further. For a correct representation of the antiprotonic emission

Table 1. Positions and half widths corresponding to antiproton (\bar{p}) and electron emission (e) and total half widths of the 2–49 resonances for $L = 12$ with and without mass polarization, given in atomic units ($a[b] = a \times 10^b$). See text for further details.

		Res. I	Res. II	Res. III
Without mass-pol.				
	Position	-195.586	-194.786	-193.628
	$\Gamma/2(\bar{p})$	7.3[-7]	8.8[-6]	2.0[-5]
	$\Gamma/2(e)$	4.4[-5]	3.6[-7]	7.7[-6]
	$\sum(\Gamma/2(\bar{p}, e))$	4.5[-5]	9.2[-6]	2.8[-5]
	$\Gamma/2(\text{total})$	5.8[-5]	9.5[-6]	3.0[-5]
With mass-pol.				
	Position	-195.586	-194.786	-193.628
	$\Gamma/2(\bar{p})$	-	1.8[-5]	3.7[-5]
	$\Gamma/2(e)$	6.2[-5]	8.5[-7]	1.3[-5]
	$\sum(\Gamma/2(\bar{p}, e))$	-	1.9[-5]	5.0[-5]
	$\Gamma/2(\text{total})$	7.8[-5]	1.9[-5]	5.3[-5]

channel and the bound part we included the maximum number of antiprotonic states in the configurations with the electronic $1s$, $2s$ and $2p$ orbitals, while for the remaining electronic orbitals only 114 antiprotonic orbitals were used. This was found to be sufficient for convergence (cf. also Fig. 3) and yields a matrix size of about $10^4 \times 10^4$.

As indicated in equation (8), not only the total width but also the antiproton ejection rate and electronic Auger rate have to be calculated distinctly in order to obtain the recombination strength. Both processes, however, arise from the electron-antiproton interaction, and it is not trivial to separate them. An approximate separation can be achieved by excluding configurations which form a certain decay channel, and as a check for consistency one can compare the sum of the hereby estimated partial widths with the obtained total width. In order to exclude Auger electron emission, only antiprotonic orbitals with $n \geq 44$ were included, so that the system becomes virtually stable against electron emission because of the absence of low lying antiprotonic states. On the other hand, to isolate the electron emission channel the low lying antiprotonic states should definitely be included, while now all configurations involving the electronic $1s$ orbital are excluded so that the system is virtually stable against emission of the antiproton. All calculations were performed with and without the mass polarization term to investigate its significance. The results are shown in Table 1.

It is found that the antiproton ejection rate of the highest 2–49 resonance is very low and could not be resolved properly in the present calculation. The result after including mass polarization is below the achieved numerical accuracy and is therefore not given in the table. The two other resonances, however, are broader and can be described rather well. The effect of the mass polarization term is clearly visible and should not be neglected even for rather heavy nuclei. The reason is of course that even compared to the large mass of a heavy nucleus the mass of the antiproton is not negligible. The second and third resonance also show good consistency in the distinct description of the channels since the sum of the antiproton

Table 2. Partial half widths for electronic radiative transitions into the final states $|\{1s\ 49\ 11\}11\rangle$ ($\Delta L = -1$) and $|\{1s\ 49\ 13\}13\rangle$ ($\Delta L = +1$) and total radiative half widths of the 2–49 resonances from Table 1, given in atomic units ($a[b] = a \times 10^b$). The coefficients from the expansion of the doubly excited states in the basis (11) correspond to the basis states $|\{2s\ 49\ 12\}12\rangle$ (c_1), $|\{2p\ 49\ 11\}12\rangle$ (c_2) and $|\{2p\ 49\ 13\}12\rangle$ (c_3).

	$ c_1 ^2$	$ c_2 ^2$	$ c_3 ^2$	$\Delta L = -1$	$\Delta L = +1$	$\Gamma_{\text{rad}}^{\text{tot}}/2$
Res. I	0.83	0.08	0.08	8.5[-5]	8.5[-5]	1.7[-4]
Res. II	-	0.526	0.47	5.7[-4]	5.1[-4]	1.08[-3]
Res. III	0.16	0.39	0.44	4.3[-4]	4.9[-4]	9.2[-4]

ton and electron emission widths agrees rather well with the obtained total width. The observed difference arises most likely due to interference effects between the channels, underlining the approximative nature of an independent treatment.

To calculate the radiative rates, we will exploit the fact that in the expansion in the basis (11) the doubly excited states are almost completely determined by only a few basis states, namely those with $n_e = 2$, $l_e = s, p$ and $n_{\bar{p}} = 49$, $l_{\bar{p}} = 11, 12, 13$. Thus, to apply the approach described in Section 4.2 we explicitly consider the matrix element that appears in (16). For a transition of the form $|\{nl\ n''l''\} L_i\rangle \rightarrow |\{nl\ n'l'\} L_f\rangle$ it reads

$$A_r = \frac{e^2}{4\pi\epsilon_0} \frac{4}{3\hbar^4} \left(\frac{\Delta E}{c}\right)^3 (2L_f + 1) \times \left(\int P_{n'l'}(r)rP_{n''l''}(r)dr\right)^2 \left\{ \begin{matrix} L_f & 1 & L_i \\ l'' & l & l' \end{matrix} \right\}^2 \langle l'' || C^1 || l'' \rangle^2. \quad (24)$$

Compared to electronic radiative transitions, the antiprotonic ones are found to be several orders of magnitude slower. The reason is the small energy difference between the levels for small changes in the main quantum number n ($A_r \sim (\Delta E)^3$). For big changes in n , on the other hand, the transitions are suppressed by the fact that the initial and final wave functions have almost no overlap. We can therefore safely neglect the antiprotonic radiative transitions in the following. Because of dipole selection rules, only the basis states that include the electronic $2p$ orbital contribute (i.e. the basis states $|\{2p\ 49\ 11\}12\rangle$, $|\{2p\ 49\ 13\}12\rangle$), while no contribution arises from the basis state $|\{2s\ 49\ 12\}12\rangle$. We obtain distinct rates for radiative stabilization into the final product states $|\{1s\ 49\ 11\}11\rangle$ ($\Delta L = -1$ -transition) and $|\{1s\ 49\ 13\}13\rangle$ ($\Delta L = +1$ -transition) by inserting the relevant quantum numbers in equation (24) and multiplying the result with the squared expansion coefficient that corresponds to the contributing basis state. The results are shown together with the coefficients in Table 2 where the total radiative stabilization rate is approximated by the sum of both partial rates. As one can see from comparison with Table 1, the electronic radiative rates are about two orders of magnitude larger than the ones for antiproton and electron ejection.

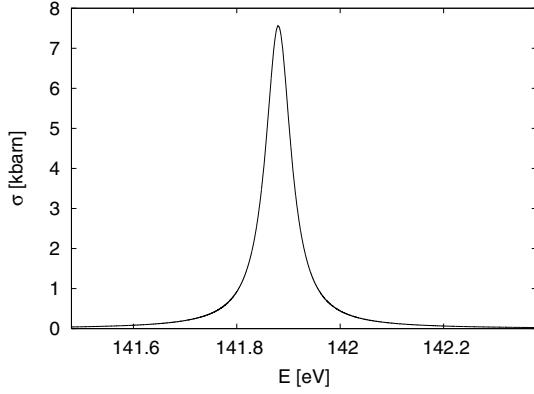


Fig. 4. Cross section for antiprotonic capture via Res. II in the isolated resonance approximation (6) as a function of antiproton energy.

4.3 Recombination strength and cross section

The calculated rates can now be used to estimate the recombination strength (8). Since the antiproton ejection width of the 2–49 resonance at -195.586 a.u. could not be resolved clearly, we will focus on the other two resonances at -194.786 a.u. (Res. II) and -193.628 a.u. (Res. III). For the chosen example, the multiplicity of the initial ion with the electron being in the $1s$ state is $g_i = 2$ due to spin, while the multiplicity of the doubly excited state d is given by its total angular momentum $L_d = 12$ and 4 possible spin couplings to $g_d = 4(2L_d + 1) = 100$. Since the radiative transitions turned out to be by far the fastest, the stabilization fraction $F_s = \sum A_{\text{stab}} / (A_a + \sum A_{\text{stab}})$ approximately equals unity ($F_s = 0.98$ for Res. II and $F_s = 0.96$ for Res. III), and the inclusion of the electronic Auger rate changes the result by only about one percent. Furthermore, we see that as long as radiative stabilization dominates (which is the case for large Z), a very precise calculation of radiative rates is not necessary since they cancel in the expression for the recombination strength. The only quantity that needs to be determined to a rather high accuracy is the antiproton ejection rate since the recombination strength is proportional to the latter. The expression for the strength can be written as $S = (\hbar^2/m_e)\xi$ where ξ is a dimensionless quantity

$$\xi = \frac{\pi^2}{2(\mu_{\bar{p}}/m_e)} \frac{\hbar A_a}{E_d - E_i} \frac{g_d}{g_i} F_s \quad (25)$$

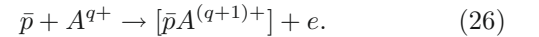
and with $\hbar^2/m_e = 7.62 \times 10^{-16}$ eV cm² we obtain $S_{II} = 7.1 \times 10^{-22}$ eV cm² for Res. II and $S_{III} = 11.7 \times 10^{-22}$ eV cm² for Res. III. The Lorentz shaped cross section profile (6) for Res. II, shown in Figure 4, has its maximum of 7.56 kbarn at 0.14 keV. Similarly, the peak for Res. III reaches its maximum of 14.06 kbarn at 0.17 keV. The widths of both resonances are much smaller than the energy distance between them and thus they can be treated as isolated to a good approximation.

5 Discussion and concluding remarks

To estimate the feasibility of resonant antiproton capture by electron excitation in highly charged ions, we adopted a theoretical approach which is based on the one often used in calculations on dielectronic recombination. The choice is motivated by the similarity of the processes. We performed illustrative calculations for a few resonances in hydrogenlike Ca^{19+} and found the cross section to be about a few kilobarn in the 0.1–0.2 keV region. The stabilization of the intermediate doubly excited electron-antiproton states is dominated by electronic radiative transitions.

The question is now how the obtained results should be interpreted with regard to the feasibility of the process in general. In principle, the calculated recombination strengths are of the same order as found in dielectronic recombination calculations and measurements, see e.g. reference [31] on lithiumlike beryllium or [32] for He^+ where the calculated strengths lie in the region $1 \leq S \leq 25 \times 10^{-22}$ eV cm². Therefore, an experimental observation of the process described in the present work does not seem impossible. Another question is whether the results can be used to draw conclusions also about ions in other charge states. The antiproton ejection rate (which is, as mentioned before, the decisive quantity) is independent of Z to a first approximation, and hence the qualitative picture is also valid for neighboring ions. However, the radiative rate scales as Z^4 which means that for lighter ions the stabilization fraction F_s can be significantly smaller than one and hence the cross section decreases. Also the electron-antiproton correlation becomes more and more significant as Z decreases. For significantly higher nuclear charge, on the other hand, relativistic effects can play a role.

Finally, there is another aspect that should be discussed. In antiproton-ion collisions, capture can also occur through a non-resonant process if an initially bound electron is scattered into the continuum:



This process has no counterpart in electron-ion recombination, although it is possible that a continuum electron is captured and a bound electron is emitted in an electron-ion collision. Such a process conserves the number of bound electrons. Contrary to this case, we are dealing with two different particles and can therefore clearly distinguish which one is emitted in the final state. The corresponding process with antiprotons (26) has been studied by Cohen for several singly charged ions [33] and by Sakimoto for He^+ [34]. The cross sections they provide are relatively large, about $\sim 0.2 a_0^2$ or ~ 5 Mbarn for a center of mass energy of 1 a.u. Note though that this is the total cross section summed over all angular momenta and over all final states of the captured antiproton, while the present calculations consider the capture into a specific quantum state. This non-resonant process is indistinguishable from the resonant process where the doubly excited state decays by electron emission. Reference [34] finds in fact that this type of resonances gives a larger

contribution than the pure direct process. This might be because the considered impact energy is such that many resonances (Rydberg series) overlap in energy and can be populated, compare e.g. the energy region of the (3–45) and (4–44) resonances in Figure 1. If the purpose is to control into which state the antiproton is captured such a resonance dense region is not an optimal choice. In highly charged ions where the energy difference between different n -manifolds is larger it might be easier to avoid them. A related question is that of interference between the resonant and non-resonant process. Such interference will of course be possible. We note however that the bulk part of the resonance strength calculated here is coming through the photon decay channel which leads to a different charge state than the direct process. With this channel no interference can take place, and thus we expect the effect of the non-resonant channel to be additive. The dominance of the photon decay channel is due to the high degree of excitation of the antiproton. To release the electron the antiproton has, for the resonances treated here, to undergo a transition with $\Delta n \geq 6$ and the result is a suppression of the Auger rate. For resonances with a higher degree of electronic excitation and a lower degree of antiproton excitation the situation can be very different.

In conclusion, we may say that from this first theoretical estimate the exotic dielectronic-like process of resonant antiproton capture in highly charged ions does not seem to be completely out of reach.

Financial support from the Swedish Science Research Council (VR) and from the Göran Gustafsson Foundation is gratefully acknowledged.

References

1. A. Lapierre et al., in *Physics with ultra slow antiproton beams*, AIP Conference Proceedings, edited by Y. Yamazaki, M. Wada (2005), Vol. 793, p. 361
2. M. Hori et al., Phys. Rev. Lett. **96**, 243401 (2006)
3. R.S. Hayano, M. Hori, D. Horvath, E. Widmann, Rep. Prog. Phys. **70**, 1995 (2007)
4. M. Iwasaki et al., Phys. Rev. Lett. **67**, 1246 (1991)
5. T. Yamazaki et al., Nature **361**, 238 (1993)
6. J.E. Russell, Phys. Rev. A **1**, 721 (1970); J.E. Russell, Phys. Rev. A **1**, 742 (1970)
7. D.E. Wright, J.E. Russell, Phys. Rev. A **6**, 2488 (1972)
8. R. Ahlrichs, O. Dumbrajs, H. Pilkuhn, H.G. Schlaile, Z. Phys. A **306**, 297 (1982)
9. V.I. Korobov, I. Shimamura, Phys. Rev. A **56**, 4587 (1997)
10. E. Widmann et al., Phys. Rev. A **51**, 2870 (1995)
11. H. Yamaguchi et al., Phys. Rev. A **70**, 012501 (2004)
12. V.I. Korobov, D. Bakalov, J. Phys. B **34**, L519 (2001)
13. O.I. Kartavtsev, D.E. Monakhov, S.I. Fedotov, Phys. Rev. A **61**, 062507 (2000)
14. J. Revai, A.T. Kruppa, Phys. Rev. A **57**, 174 (1998)
15. T. Yamazaki, N. Morita, R.S. Hayano, E. Widmann, J. Eades, Phys. Rep. **366**, 183 (2002)
16. J.S. Cohen, Rep. Prog. Phys. **67**, 1769 (2004)
17. D. Gotta, K. Rashid, B. Fricke, P. Indelicato, L.M. Simons, Eur. Phys. J. D **47**, 11 (2008)
18. H.A. Kramers, Philos. Mag. **46**, 836 (1923)
19. M. Tokman et al., Phys. Rev. A **66**, 012703 (2002)
20. R. Schioppa, Z. Harman, W. Scheid, N. Grün, Eur. Phys. J. D **31**, 21 (2004)
21. V.I. Korobov, Phys. Rev. A **67**, 062501 (2003); V.I. Korobov, Phys. Rev. A **68**, 019902(E) (2003)
22. C. de Boor, *A practical Guide to Splines* (Springer, New-York, 1978)
23. H. Bachau, E. Cormier, P. Decleva, J.E. Hansen, F. Martin, Rep. Prog. Phys. **64**, 1815 (2001)
24. E. Lindroth, J. Wallenius, S. Jonsell, Phys. Rev. A **68**, 032502 (2003)
25. J.L. Sanz-Vicario, E. Lindroth, N. Brandefelt, Phys. Rev. A **66**, 052713 (2002)
26. T. Yamazaki, K. Ohtsuki, Phys. Rev. A **45**, 7782 (1992)
27. I. Shimamura, M. Kimura, Phys. Rev. A **50**, 5346 (1994)
28. I. Shimamura, Phys. Rev. A **46**, 3776 (1992)
29. I. Lindgren, J. Morrison, *Atomic Many-Body Theory* (Springer, 1986)
30. A.R. Barnett, Comput. Phys. Commun. **21**, 297 (1981)
31. T. Mohamed et al., Phys. Rev. A **66**, 022719 (2002)
32. D.R. DeWitt, E. Lindroth, R. Schuch, H. Gao, T. Quinteros, W. Zong, J. Phys. B **28**, L147 (1995)
33. J.S. Cohen, Phys. Rev. A **69**, 022501 (2004)
34. K. Sakimoto, Phys. Rev. A **74**, 022709 (2006); K. Sakimoto, Phys. Rev. A **76**, 042513 (2007)